# Direct observation and modelling of embolism spread between xylem conduits: a case study in Scots pine.

Running title: Embolism formation and spread in Scots pine

José M. Torres-Ruiz[1*], Hervé Cochard[2], Maurizio Mencuccini[3,4], Sylvain Delzon[1], Eric Badel[2]

*Author for correspondence:

*José M. Torres-Ruiz.*

Contact details: Telephone: +330540006973; Email: torresruizjm@gmail.com; Address: BIOGECO, INRA, Univ. Bordeaux, 33615 Pessac, France

[1] BIOGECO, INRA, Univ. Bordeaux, 33615 Pessac, France.

[2] PIAF, INRA, Univ.Clermont Auvergne, 63000 Clermont-Ferrand, France.

[3] School of Geosciences, University of Edinburgh, Crew Building, The Kings Buildings, West Main Road, EH93JF Edinburgh, UK.

[4] ICREA at CREAF, 08193, Cerdanyola del Vallès, Barcelona, Spain

Number of words main body (Introd., Methods, Results, Discussion and Conclusions): 5825

Figures: 8.

Tables: 1.

Supporting information: 2 figures, 1 video.

# Abstract

Xylem embolism is one of the main processes involved in drought-related plant mortality. Although its consequences for plant physiology are already well described, embolism formation and spread are poorly evaluated and modelled, especially for tracheid-based species. The aim of this study was to assess the embolism formation and spread in *Pinus sylvestris* as a case study using X-ray microtomography and hydraulics methods. We also evaluated the potential effects of cavitation fatigue on vulnerability to embolism and the micro-morphology of the bordered pits using Scanning electron microscopy (SEM) to test for possible links between xylem anatomy and embolism spread. Finally, a novel model was developed to simulate the spread of embolism in a 2D anisotropic cellular structure. The results showed a large variability in the formation and spread of embolism within a ring despite no differences being observed in intertracheid pit membrane anatomical traits. Simulations from the model showed a highly anisotropic tracheid-to-tracheid embolism spreading pattern, which confirms the major role of tracheid-to-tracheid air seeding to explain how embolism spreads in Scot pine. The results also showed that prior embolism removal from the samples reduced the resistance to embolism of the xylem and could result in overestimates of vulnerability to embolism.

The submitted manuscript addresses, by using X-ray microtomography and hydraulic methods, a relevant and poorly evaluated question in plant physiology: the embolism formation and spread among xylem conduits in Scots pine as a case study. Results showed a large variability in embolism resistance within a single ring despite no anatomical differences were observed in those traits associated with resistance to embolism between tracheids. Indeed, and for the first time in a tracheid-based species, an increased vulnerability to embolism was observed in tracheids that were embolised once, confirming the occurrence of cavitation fatigue in conifers. Finally, a novel model was developed to simulate how embolism spreads among tracheids, allowing us to confirm the major role of the tracheid-to-tracheid air seeding in the xylem embolism spreading in Scot pine.

## Introduction

In plants, water moves through the xylem under metastable conditions due to the tension induced by its evaporation at the leaf surface. This tension allows its transport from soil to leaves but also favours the occurrence of cavitation events in xylem conduits, i.e. the change from liquid to water vapour (Dixon & Joly 1895; Tyree &Sperry 1989). Cavitation results in the appearance of embolism that provokes the hydraulic dysfunction of the xylem and reduces plant water transport capacity. During water shortage, reductions in soil extractable water increase xylem tension and, therefore, cause the occurrence of cavitation events. Xylem embolism is considered one of the principal mechanisms causing drought-related mortality in woody species (Brodribb & Cochard 2009; Brodribb *et al.* 2010; Urli *et al.* 2013; Anderegg *et al.* 2015), explaining why evaluating plant resistance to embolism both across and within species has received considerable attention during the last decades (Cochard *et al.* 2013 and 2016; Torres-Ruiz *et al.* 2013). However, whereas most of the studies have been focused on the consequences of hydraulic dysfunction for plant physiology and survival, less attention has been paid to embolism spread from conduit to conduit despite its relevance for a better understanding of plant functioning. This knowledge gap has been mostly caused by the lack of access to non-invasive techniques that allow the direct observation of the xylem lumen content and, therefore, the high-resolution quantification of embolism (Cochard *et al.* 2015). The access to synchrotron facilities and the emergence of desktop-based X-ray microtomography (micro-CT) systems have favoured the first evaluations of embolism spreading in plants, reporting a good agreement between hydraulic

and micro-CT results (Choat *et al.* 2016). Thus, by using these techniques, Brodersen *et al.* (2013) reported for *Vitis vinifera* that embolism appears first in xylem vessels surrounding the pith and, as water potential decreases, spreads radially towards the epidermis. On the contrary, Choat *et al.* (2015) reported that embolism in *Sequoia sempervirens*, a tracheid-based species, appears by describing three different patterns: in wide tangential bands of tracheids, as isolated tracheids and as functional groups connected to leaves. Dalla-Salda *et al.* (2014), however, reported that embolism in Douglas-fir (*Pseudotsuga menziesii* (Mirb) Franco) initiates and propagates successively at two different xylem locations: first in the latewood and then in the earlywood. Finally, Knipfer *et al.* (2015) showed that embolism in *Juglans microcarpa* appeared initially in isolated vessels and then spread to multiple vessels in close proximity. Despite the differences among studies in their reported embolism spreading patterns, all they agree in that the primary mechanism causing embolism spread is air seeding. The different patterns described up to date reflect an important variability in how embolism initiates and spreads among plant species. However, a dedicated model able to describe such differences is still missing.

Air seeding is defined as the aspiration of gas into functional conduits from adjacent embolised ones (Zimmermann & Brown 1971; Sperry & Tyree 1988). The structure and characteristics of the inter-conduit pits have an important role in avoiding the spreading of drought-induced embolism since they determine the pressure gradient required for the rupture of the air-sap meniscus and, therefore, embolism propagation through their pits (Tyree & Zimmermann 2002; Lens *et al.,* 2013). In angiosperms, two adjacent vessels are separated by a porous pit membrane which traps air-water menisci and avoids air leaks when xylem tension increases. In conifers, inter-tracheid pits are morphologically different and they act as valves to block the air spreading from embolised to functional tracheids. They consist of circular bordered pits with a centrally located torus that is passively aspirated to the aperture

of the pit chamber. Whereas in angiosperms the air seeding depends on the size of the largest pores in the pit membranes separating two vessels (Choat *et al.* 2003; Christman *et al.* 2009), the more complex structure of the inter-tracheid pits in conifers makes it depends on the adhesion of the torus to the pit border, as the seal capillary-seeding hypothesis suggests (Delzon *et al.* 2010). A recent survey of 115 conifer species by Bouche *et al.* (2014) showed how the ratio of torus to pit aperture diameter, i.e., the torus overlap, increases with increasing embolism resistance of the species, suggesting that air-seeding is located at the seal between the aspirated torus and pit aperture. The patterns of embolism spreading among tracheids would also be therefore related to differences in pit anatomy that generate differences in torus/pit aperture overlap. However, information on the dynamics of embolism spreading among tracheids depending on their pit anatomy characteristics is virtually non-existent.

During the last few years, the identification of different sources of artefacts that may affect the accuracy of the results in plant hydraulics has led to a revision of the methods and protocols used to construct vulnerability curves (Cochard *et al.* 2010, 2013; Sperry *et al.* 2012; Wheeler *et al.* 2013; Torres-Ruiz *et al.* 2014, 2015). One of the possible sources of bias that has poorly been evaluated is the use of samples from which embolisms had previously been removed. Prior embolism removal can make xylem conduits appear more vulnerable to embolism due to the phenomenon of 'cavitation fatigue' (Hacke *et al.* 2001). Cavitation fatigue has been related to changes in the pressure difference required for gas-aspiration from an embolised conduit into a functional one, being linked with changes both in the stretching and deflection capacity of the pit membrane in angiosperms as well as with the seal capacity (Delzon *et al.* 2010) and elastic stretching properties of the torus in gymnosperms (Stiller & Sperry 2002). The cavitation fatigue phenomenon causes embolism spread to take place at lower xylem tensions among those conduits that have been embolised at least once,

underestimating therefore resistance to embolism. Although the relevance of cavitation fatigue '*in vivo*' is not clear because of the uncertainties about the capacity of the plants to refill embolised conduits while the xylem is under tension (Delzon & Cochard 2014; Cochard *et al.* 2013; Charrier *et al*. 2016), fatigue can have an important influence in affecting vulnerability curves from embolism-removed xylem samples.

By both direct and indirect xylem observation, the mains aims of this study were to evaluate (i) the within-ring variability pattern in embolism resistance and spread, and (ii) how the prior embolism removal from tracheid-based xylem samples could affect the resulting vulnerability curves in current-year branches of Scots pine (*Pinus sylvestris* L.), one of the most well-understood model tree species with regard its hydraulic properties (Mencuccini & Grace 1996; Martinez-Vilalta *et al.* 2009; Sterck *et al.* 2012; Salmon *et al*. 2015). Indeed, we also analysed the micro-morphological characteristics of the bordered pits to determine if the observed spreading patterns are related not only to differences in the anatomical traits associated with resistance to embolism, but also to the presence of isolated embolised tracheids. The results are used to parameterise a novel model to predict embolism formation and spreading along xylem conduits and explain the spatial patterns observed by direct visualization. Furthermore, by using both micro-CT and hydraulic techniques, we evaluated how prior embolism removal from the xylem samples could affect the resulting vulnerability curves.

## Material and methods

**Direct observation of embolism spreading.**

Embolism spreading was evaluated in three current-year branches from three different individuals of Scots pine located in the vicinity of the INRA-Crouel campus in Clermont-

Ferrand (France). Sampled branches were 0.5 to 1 cm in diameter and ca. 40 cm in length, and they all were located in full sunlight-exposed conditions. Samples were collected during the morning, wrapped into plastic bags with wet paper towel inside for at least 2 h (to minimise transpiration and promote equilibration between needle and xylem water potential of the stem, $\Psi_n$ and $\Psi_x$ respectively), and their $\Psi_x$ were determined with a Scholander chamber on 3-4 needles per branch. Samples were then adjusted to 150-mm length with a razor blade and placed in an X-ray microtomograph (Nanotom 180 XS, GE, Wunstorf, Germany) at the PIAF laboratory (INRA, Clermont-Ferrand, France) to determine the amount of native embolisms by evaluating three-dimensional images of the internal structure of the sample. For the micro-CT image acquisition and image combination, the field of view was fitted to $4.0 \times 4.0 \times 4.0$mm and the X-ray source set to 50 kV and 275 $\mu$A. For each 42-min scan, 1000 images were recorded during the 360∘ rotation of the sample. After 3D reconstruction, the spatial resolution of the image was $2.00 \times 2.00 \times 2.00$ $\mu$m per voxel. One transverse 2D slice was extracted from the middle of the volume using VGStudio Max© software (Volume Graphics, Heidelberg, Germany). As embolisms cannot be removed in conifer xylem samples by flushing water at high pressure because of the torus margo sealing, samples were vacuum infiltrated in 10 mM KCl solution for a minimum of eight hours to promote such embolism removal (previous observations by using micro-CT showed that this time was sufficient to remove all the embolisms). Vacuum infiltration is considered a viable and verifiable alternative to flushing for removing embolism in tracheid-based conducting systems since it reduces the risk of pit aspiration and of clogging the cut end (Hietz *et al.* 2008). Samples were inserted in a 150-mm-diameter custom-built rotor designed according to Alder *et al.* (1997) and spun for 5 minutes at increasing speeds to get progressively higher xylem tensions up to 3.0 MPa, corresponding to the xylem water potentials typically reached by the species at its range boundary in the Mediterranean basin (e.g., ca. -2.5 MPa in Poyatos

*et al.* 2013; ca. -2.1 MPa in Salmon *et al.* 2015). Thus, the following tensions were induced in the middle of the samples by spinning: 0.5, 1.0, 1.5, 2.0, 2.5 and 3.0 MPa. After each spinning, samples were removed from the rotor and scanned to visualize the embolism induced at each tension in the centre of the sample. This first set of xylem tensions induced in the samples will be referred to as 'first cycle of embolism' from now on. After the last scan, i.e. after inducing at tension of 3.0 MPa, samples were vacuum infiltrated again (for a minimum of eight hours) to allow the complete refilling of the conduits. Samples were then subjected to the same xylem tensions and scanned again in the micro-CT for a second time and at the same point to ensure an exact 3D overlap of the two scans (referred to as 'second cycle of embolism' from now on). The amount of embolisms formed at each xylem tension was determined as described below and compared between the first and second cycle of embolism. All samples were wrapped into a paraffin film before each scanning to prevent drying during X-ray scans.

The dynamics of xylem embolism spreading was evaluated in the centre of the sample by adjusting to the field of view of the scanner in order to avoid boundary artefacts related to the width of the branches. The scanned xylem area was divided into five equal sections from the limit of the pith (section 1) to the beginning of the bark (section 5) (Supporting information Fig. S1). As previous observations reported non-significant differences in tracheid diameter between the xylem sections, the percentages of embolised tracheids (%) of each section and of the entire portion at each tension were then calculated similarly to Choat *et al.* (2015), i.e. by comparing the area of observed functional and embolised xylem area ($A_f$ and $A_c$ respectively) as:

$$\text{Percentage area of embolised tracheids} = (A_c \times 100) / (A_c + A_f)$$

To evaluate a possible effect of prior embolism removal on the resulting vulnerability curves, the percentage of embolised tracheids in each section and in the entire sample area were compared at each tension during the first and second embolism cycle. The dynamics of embolism spread between the different sections was also evaluated during both cycles to detect possible changes in the spreading patterns.

By combining micro-CT images we detected and located the tracheids that become embolised when xylem tension increased from 2.0 to 2.5MPa during the first cycle of embolism. Being focused on these embolised tracheids, we removed the embolism by vacuum infiltration and determined the percentage of them that become embolised at a lower xylem tension than during the first cycle (i.e. 2.0 MPa or lower). This allowed us to calculate the percentage of tracheids that reduced their resistance to embolism once they had been embolised once (% of fatigued conduits). To ensure that these tracheids were not already influenced by previous embolism events, only those tracheids of the current-year branches that were fully functional when samples were collected (i.e., under native conditions) were considered for these calculations.

**Modelling embolism formation and spatial spreading (SimCav software)**

A numerical model (SimCav) was developed to simulate transversal embolism spreading in a 2D cellular structure. The outputs of the model are images that describe the pattern of embolised and non-embolised cells in the material. The 2D model works as follows: As a basis material, we used a representative transversal area made of 900 (30x30 in radial and tangential direction) square cells equivalent in size to the original images obtained by micro-CT analysis. The square tracheids are organized in radial columns and tangential lines that

mimic the transversal structure of the xylem of gymnosperms. Each tracheid is connected to four neighbouring tracheids; two in the radial direction and two in the tangential direction. Then, starting from this non-embolised cellular structure, the model virtually increases the xylem tension and indicates the cells that become embolised at a given tension. The number of embolised tracheids is driven by the experimental vulnerability curve that fixes the percentage of tracheids that become embolised at each xylem tension. Thus, the parameters of the vulnerability curve derived from adjusting the Pammenter & Vander Willingen (1998) equation were included in the model. At this step, several cases are possible to explain embolism formation and spreading: i) a tracheid may become embolised despite being surrounded by water-filled (i.e. functional) tracheids. This behaviour acts as a spatially random process in the 2D cross section. Alternatively, a tracheid may become embolised because it is connected to an already embolised tracheid and then becomes embolised by air-seeding. In this case, the spreading occurs either in ii) the radial or iii) the tangential direction according to the orientation of the common cell wall. These three scenarios represent the three processes by which a cell can becomes embolised. For each process is given a probability of occurrence that can be adjusted by two parameters: i) the "cell-to-cell Spreading" to "Random emergence" ratio (SR) that indicates how much a non-embolised tracheid connected to an embolised one is more sensitive to an embolism event relative to a random event; ii) the "Anisotropic Spreading" ratio (AS) indicates a preferential spreading along either the radial or the tangential direction. Thus, an AS equals to 2 means that, in case of spreading, the probability of radial spreading is 2 times higher than tangential spreading. The names 'air-seeding' and 'homogeneous nucleation' are avoided here because the two-dimensional nature of the model precludes direct inference on the causes of embolism emergence. According to these embolism assumptions (random emergence, more or less anisotropic spreading), the model generates the embolism pattern in the cells network for

each xylem tension (see the movie S3). The output is given as a 2D picture, for each step, of the embolism pattern of the cellular structure. A snapshot of the computing interface of the software is given as a supplementary material (S2).

The model was parameterized by using micro-CT observations. The model was run using a wide range of SR and AS values; SR ranged from 0 (fully random process) to 10 and AS ranged from 1 (isotropic spreading) to 30. The resulting simulations depicted the wide range of possibilities, from a totally random to a very isotropic or anisotropic embolism spreading pattern. Then, we compared the simulated pattern with results from an experimental micro-CT scan, both fixed at 30% of embolised cells. The agreement between simulated and experimental images was computed by counting the number of cell-to-cell connexions in the radial (CR) and the tangential (CT) directions, and the number of isolated embolised cells (IC) and calculating the root-mean-square error:

$$\text{error} = \sqrt{\frac{\left(CR_{sim} - CR_{exp}\right)^2 + \left(CT_{sim} - CT_{exp}\right)^2 + \left(IC_{sim} - IC_{exp}\right)^2}{N_{total}}} \qquad \text{eq. 1}$$

with $N_{total}$ indicating the total number of connexions. For model validation, the resulting fitted parameters were used to simulate the spreading patterns at 60% of embolised cells and results compared with real patterns obtained from micro-CT scans for such percentage of embolised tracheids.

**Effect of embolism removal on resulting vulnerability curves**

In addition to results obtained by direct observation (i.e. micro-CT), the influence of prior embolism removal was also evaluated hydraulically by using the flow-induced centrifugation technique (Cavitron: Cochard *et al.* 2002, 2005). To eliminate inter-individual variability, current-year branches were collected from a single Scots pine individual. Briefly, three ca.60 cm-long branches were sampled early in the morning, doubled-bagged in plastic bags and transported to the lab. A 280 mm-long current-year segment per branch was then excised by carrying out several cuttings under water, debarked to minimize resin exudation and both ends trimmed with a fresh razor blade. Each sample was installed in a 280-mm-diameter custom-built honeycomb rotor (Lamy *et al*. 2011) and its maximum hydraulic conductance determined under low xylem tension (i.e. close to zero). The speed of rotation was then gradually increased to induce different xylem tensions and the percentage loss of hydraulic conductance (PLC) calculated by measuring the hydraulic conductance after each tension until reaching 100% PLC. After obtaining a vulnerability curve for each sample (first cycle of embolism curves), all segments were vacuum infiltrated for a minimum of eight hours and a second curve generated from the same samples (second cycle of embolism curves). All measurements and the vacuum infiltration were done by using a degassed and ultrapure 10 mM KCl and 1 mM CaCl2 solution. Both curves were fitted using the equation provided by Pammenter & Vander Willigen (1998):

$$PLC = \frac{100}{1+e^{a(\Psi-b)}} \quad , \qquad \qquad \text{eq. 2}$$

with *a* representing a dimensionless parameter controlling the shape of the curve and *b* the xylem tension for a loss of hydraulic conductance of 50% ($P_{50}$).

**Micro-morphology of bordered pits**

Differences in the morphology of the bordered pits can result in different capacities to avoid seal capillary seeding. To check if the patterns of embolism spreading among tracheids are related to morphological differences of their bordered pits, the torus overlap ($O$), the margo flexibility ($F$) and the valve effect ($V_{EF}$) were determined in tracheids located both in the more intermediate (xylem sections 2, 3 and 4) and outer (sections 5, see Fig. S1 in supporting information) parts of the xylem of four current-year branches. The relevance of the so-called 'valve effect' is due to its role in the avoidance of the air spreading into the functional tracheids (i.e. in embolism resistance) and it depends on the torus diameter relative to pit aperture diameter. Measurements were carried out by using scanning electron microscopy (SEM, PhenomG2 pro; FEI, The Netherlands) at the Caviplace platform (INRA - University of Bordeaux) as described in Bouche *et al.* (2014, 2016). Briefly, 5-8 mm-long samples were cut with a razor blade in the radial direction, dried for 48 h at 70 °C, coated with gold for 40 s at 20 mA (108 Auto; Cressington, UK) and observed under 5 kV. The $O$, $F$ and $V_{EF}$ were then calculated as described by Delzon *et al.* (2010):

$$O = \frac{(D_{TO} - D_{PA})}{D_{TO}} \qquad \text{eq.3}$$

$$F = \frac{(D_{PM} - D_{TO})}{D_{TO}} \qquad \text{eq.4}$$

$$V_{EF} = F \; x \; O \qquad \text{eq.5}$$

being $D_{TO}$, $D_{PA}$ and $D_{PM,}$ the torus, pore aperture and pit membrane diameters, respectively. A minimum of 60 bordered pits were analysed in each sample (30 pits in the intermediate sections and 30 pits in the outer one). All SEM images were analysed with ImageJ freeware (Rasband 2014).

**Statistical analyses**

Statistical analyses were carried out using Sigmaplot (SPSS Inc., USA). Differences in mean torus area, pore area, $O$, $F$ and $V_{EF}$ values between those xylem sections located between the inner and outer parts of the xylem, and the outer part of the xylem were evaluated by Student t-test. Similarly, the mean xylem tension inducing 50% loss of hydraulic conductance (Cavitron) or 50% of tracheid area embolised (both for the entire xylem portion and for each xylem section by using micro-CT; Table 1) between first and second cycle of embolism were evaluated by paired t-tests. Statistical comparisons were considered significantly different at $p<0.05$. All data sets were previously tested for distributional normality and variance homogeneity.

# Results

Measurements of the native embolism in the Scots Pine samples showed a percentage of embolised tracheid area of 22.2%, being most of them located either in the inner (section 1) or the outer section (section 5) of the xylem (Fig. 1c). During the first cycle of embolism, most of the embolism observed at relatively low xylem tensions (<1.5 MPa) were located in these two sections (Fig. 1a). Only when xylem tensions reached values above 1.5 MPa, did embolism start to spread to the more intermediate xylem sections (i.e., sections 2, 3 and 4). A similar spreading pattern occurred during the second cycle of embolism. Thus, the embolised area increased first in the inner (near the pith) and outer (near the bark) sections and then, as the xylem tension increased, in the more intermediate ones (Fig. 1b). However, the percentages of embolised tracheids in the intermediate sections were higher during the second cycle than during the first one for all the xylem tensions evaluated.

The high spatial resolution of the micro-CT images allowed evaluation of the embolism spreading at conduit level. Thus, the combination of micro-CT images from two consecutively induced tensions, i.e. 2.0 and 2.5 MPa, showed that an important amount of the tracheids that became embolised at 2.5MPa were connected to an embolised tracheid at 2.0MPa, suggesting both a tangential and radial embolism spreading along neighbouring tracheids (Fig. 2). Apart from the spreading along adjacent tracheids, isolated embolised tracheids (i.e., surrounded by functional tracheids) were also observed in 2D transverse and tangential images as xylem tension increased (Fig. 2c). However, when 3D re-constructed images were analysed, some of such apparently isolated tracheids appeared to be actually connected to other embolised tracheids but at a different height (Fig. 3).

The parametrization of the model at PLC=30% allowed determination of the best input parameters (SR and AS) to explain the observed embolism pattern by minimizing the difference between simulated and experimental images with a root-mean-square error equal to 0.2 (Fig. 4). The results showed how anisotropic spreading is the dominant process in the observed embolism spreading patterns. Thus, the optimal AS value was 8 which means that the radial spreading is 8 times more frequent than the tangential one. The optimal SR was ca. 2, indicating that the probability of "spontaneous" (or "random") embolism to occur is two times lower than the tangential (and 16 times lower than radial spreading). The comparison between results from the model and experimental x-ray tomographic images at 60% of embolised tracheids revealed a very small difference in terms of the distribution of cell-to-cell connections (according to eq.1) with a root-mean-square error of 1.02. This shows therefore the robustness of the approach and confirms that the fitted values for AS=8 and SR=2 provide realistic xylem embolism patterns (Fig. 5).

The micro-morphological analysis of the bordered pits showed significant differences in torus and pore sizes between the outer and the more intermediate sections of the xylem. Thus, whereas tracheids in the outer section of the xylem showed mean torus and pore areas of 21.0 and 8.8 $\mu m^2$ respectively, they reached 35.6 and 15.6 $\mu m^2$, respectively, in the intermediate sections (Fig. 6). Despite these morphological differences in their pit membranes, tracheids from the outer and the more intermediate xylem areas showed similar values in torus overlap, margo flexibility and valve effect, i.e., those traits related to resistance to embolism.

Results from the micro-CT image analyses suggested that vulnerability to embolism of the embolism-removed samples increased slightly when these samples were exposed to high xylem tensions for a second time. The apparent increase was confirmed hydraulically by using the Cavitron. Thus, micro-CT images showed that the xylem tension required to embolize 50% of the xylem tracheid area decreased from $3.02 \pm 0.13$ MPa to $2.55 \pm 0.14$ MPa in embolism-removed samples (Fig. 7a, Table 1). This decrease was observed in most of the xylem sections, being significant in the intermediates ones (Table 1). Results from the Cavitron confirmed these observations showing that $P_{50}$ decreased significantly, from $3.30 \pm 0.12$ MPa to $2.76 \pm 0.32$ MPa, during the second cycle of embolism induction (Fig. 8, Table 1). Across tracheids, results from the combined micro-CT images also revealed a shift in the resistance to embolism between the two cycles of embolism induction (Fig. 7b). Thus, $81.3 \pm 5.9\%$ (mean $\pm$ standard error, $n=3$) of the tracheids that became embolised when the xylem tension increased from 2.0 to 2.5 MPa during the first cycle of embolism, appeared already embolised at a xylem tension of 2.0 MPa during the second cycle. This, therefore, indicates a reduction in resistance to embolism in those tracheids that had been embolised once.

## Discussion

Direct micro-CT observations revealed that tracheids do not embolize homogeneously along the entire xylem tissue in *Pinus sylvestris* but progressively from inner and outer xylem areas to the intermediate ones. Micro-CT scans showed how tracheids become embolised at lower xylem tensions near the pith and the bark than in the intermediates parts of the xylem. Xylem areas near the pith and close to the bark are, therefore, responsible for most of the hydraulic conductance losses observed at relatively low xylem tensions (i.e. up to 1.5 MPa). As xylem tension increases, embolism propagates to the intermediate regions of the xylem. It is important to mention that a fraction of the air-filled tracheids observed near the pith at low xylem tensions might be caused not directly by the spreading or induction of embolism, but by the destruction by stretching of protoxylem as a consequence of plant growth (Rockwell *et al*. 2014). These air-filled protoxylem conduits represent a potentially important source of air that could facilitate the entry of air into other xylem areas and, therefore, would explain the radial embolism spreading from the pith previously observed in this and other angiosperms species (e.g., *Vitis vinifera*, Brodersen *et al*. 2013). The presence of air in the pith is very common in intact plants (e.g. in *Eucalyptus pauciflora* at a xylem tension of 3.6MPa, Torres-Ruiz *et al*. 2015), even when they show relatively low xylem tension values (e.g., in *Helianthus annuus* at 0.4 MPa, Torres-Ruiz *et al*. 2015). In fact, scans obtained from samples which showed relatively low native hydraulic conductance losses (PLC=22.2%) revealed that an important amount (41.35%) of the already embolised tracheids were located in the innermost xylem areas. Similarly, the presence of air in the bark could also works as a source of air that can facilitate air seeding. However, the exposure to air of the outer and inner tracheids cannot only explain the observed embolism pattern since higher xylem tensions are required to increase the percentage of embolised tracheids in the most intermediate xylem areas, what supports the vulnerability segmentation hypothesis among tracheids.

Across tracheids, micro-CT images revealed that embolism spreads both tangentially and radially. The radial propagation was unexpected considering that most of the tracheid bordered pits are located in the radial walls (Mauseth 1988), a fact that theoretically would favour a tangential occurrence of the air-seeding. This partly agrees with Choat *et al.* (2015) who also observed a tangential embolism spreading in *Sequoia sempervirens,* but not a radial one as observed here for Scots pine. Simulations from the model confirmed that a purely random or isotropic embolism spreading cannot explain the observed embolism pattern with micro-CT. Interestingly, the model showed that the probability for embolism to spread radially is 8 times higher than for a tangential spreading. In addition, the model also showed that the probability for embolism to spread cell-to-cell is 18 times higher than for the occurrence of isolated embolization events, confirming therefore the major role of tracheid-to-tracheid air seeding in explaining the observed embolism spreading in Scot pine. The preferential radial spreading could be due to differences in the micro-morphological characteristics of the bordered pits located on the radial walls relative to those on the tangential walls of the tracheids. Despite their reduced numbers, the bordered pits on radial walls may be less effective at avoiding air-seeding. Also, radial spreading could be related with the characteristics of the bordered pits located at the tips of the tracheids since, in conifers, bordered pits are not homogeneously distributed along the entire tracheid length, showing a higher density towards the tips (Sirviö and Kärenlampi 1998). These tracheids tips bend and overlap rather than abut (Becker *et al.* 2003; Philippe *et al.* 2010) which would favour the change in orientation of the radial walls to the tangential direction and, therefore, the radial spreading of the embolism. The fact that radial embolism spreadings were detected in *P. sylvestris* but not in *S. sempervirens* could be related with differences in their xylem anatomy, e.g. *S. sempervirens* shows wider tracheids (13.8-μm-diameter tracheids in average, Burgess *et al.* 2006) than *P. sylvestris* (5.5-μm-diameter tracheids in average, this study),

although more anatomical studies on tracheids are required to confirm this hypothesis. It is important to highlight that when 3D images were analysed, some of the supposedly isolated tracheids observed in 2D transverse and tangential sections were not totally surrounded by functional conduits, but actually connected with other embolised ones at a different height. Thus, the "random" process, which has been quantified by the model to be very rare in a 2D transversal cross section, could also result from cell-to-cell spreading but at a different height. The different embolism patterns observed in gymnosperms (Dalla-Salda *et al.* 2014; Choat *et al.* 2015; this study) highlight the importance of studying different model species as Scot pine for the proper understanding of how embolism spreads in tracheid-based trees.

The fact that the inner and outer tracheids become embolised earlier, i.e., at lower xylem tensions, compared to those located in intermediate xylem areas, indicates a certain degree of vulnerability segmentation (Tyree *et al.* 1993; Tsuda & Tyree 1997) among tracheids located in the same ring. According to the air-seeding hypothesis, such segmentation at tracheid level would be related to differences in the air-seeding threshold required to pull air into a functional tracheid from an embolised one and, therefore, with the morphological characteristics of bordered pits. However, our micro-morphological analyses showed no differences in those traits related with seal capillary-seeding (i.e., torus overlap, margo flexibility and valve effect) between tracheids located in the outer and intermediate parts of the xylem despite their showing significant differences in both torus and pore area. Whereas those traits are good proxies for estimating embolism resistance across conifer species (Bouche *et al.* 2014), our results showed how they cannot explain the differences in embolism resistance observed among tracheids within a ring. This is consistent with previous studies relating differences in resistance to embolism with the different stretching capacities of the pit membranes more than with bordered pits characteristics (Domec *et al.* 2006). However, all micro-morphological analyses were carried out on bordered pits located at

tangential tracheid walls so, given the observed radial embolism spreading, further analyses including the few tracheids at the radial walls and the evaluation of the diameters of their margo pores would be required to explain the observed vulnerability segmentation.

Vulnerability curves obtained hydraulically (Cavitron) confirmed the reduction in embolism resistance observed using micro-CT in embolism-removed samples when they were exposed to high xylem tensions for a second time. These reductions make samples more prone to become embolised again at lower xylem tensions and, therefore, would underestimate the resistance to embolism of the species when embolism-removed samples are used for generating vulnerability curves. The reduction in embolism resistance was also confirmed at single conduit level by combining successive micro-CT images. This allowed us to detect and localize which tracheids became embolised at a lower xylem tension during the second cycle of embolism compare with the first one. To our knowledge, this work is the first evidence of the occurrence of the 'cavitation fatigue' phenomenon not only at conduit level, but also in tracheid-based xylem samples, highlighting the importance of using native xylem samples (i.e., without removing native embolisms) for determining resistance to embolism accurately. This links with the importance of quantifying sample native embolism by using micro-CT observations prior to the generation of a vulnerability curve to check if it is low enough for a truthful representation of the sample resistance to embolism. Although this study was not concerned with the causes of the reductions in embolism resistance, cavitation fatigue has typically been related with changes in the air-seeding pressure due to a stretching or degradation of the pit membranes during previous embolism events. A possible cause could also be the nanobubbles remaining in xylem conduits after removing the embolisms (Schenk *et al.* 2015). Despite reductions in embolism resistance, embolism spread showed similar spatial patterns during the first and the second cycles of embolism, indicating that such reductions occurs similarly in all tracheids independently of their location in the xylem

tissue. Also, it is unlikely to be caused by torus rupture since that would have resulted in a drastic decrease in the resistance to embolism during the second cycle of embolism. Although our results show a clear effect of embolism removal on the resulting vulnerability curves in excised xylem segments, more studies are required to determine if there is also an effect on 'in vivo' intact plants, especially considering the debate about the occurrence of refilling and embolism-removal capacity of plants on a daily basis (Delzon & Cochard 2014; Cochard *et al.* 2015; Sperry 2013; Charrier *et al.* 2016).

## Conclusions

Our results showed that, at low xylem tensions, embolised tracheids in Scots pine branches are located mostly in the inner and outer xylem areas (i.e., located near the pith and the bark respectively). Then, embolism spreads to the more intermediate xylem regions as tension increases, indicating a certain level of vulnerability segmentation within xylem areas. Interestingly, this segmentation was not related to differences in the morphological characteristics of the bordered pits, as found instead for the differences in resistance to embolism across conifer species. Simulations from the presented model showed that the probability for embolism to spread radially is higher than for a tangential spreading, and that the cell to cell embolism spreading is much more frequent than the occurrence of isolated embolization events. Results also showed, for the first time in a tracheid-based species and at conduit level, how the prior embolism removal from xylem sample increases artificially the vulnerability to embolism of the plant material, favouring the generation of biased vulnerability curves that would underestimate the resistance to embolism. Therefore, samples without prior removal of embolisms should be used for the proper evaluation of the resistance

to embolism but, at the same time, with low native PLC levels to ensure both the truthfulness and representativeness of the results.


## Acknowledgments

# References

Alder N.N., Pockman W.T., Sperry J.S. & Nuismer S. (1997) Use of centrifugal force in the study of xylem cavitation. *Journal of Experimental Botany* 48, 665–674.

Anderegg W.R.L, Flint A., Huang C., Flint L., Berry J.A., Davis F.W., Sperry J.S. & Field C.B. (2015) Tree mortality predicted from drought-induced vascular damage, *Nature Geoscience* 8, 5, 367

Becker P., Gribben R.J. & Schulte P.J. (2003) Incorporation of transfer resistance between tracheary elements into hydraulic resistance models for tapered conduits. *Tree Physiology* 23, 1009–1019.

Bouche P.S., Delzon S., Badel E., Burlett R., Cochard H., Lavigne B., Mayr S., Zufferey V., Choat B., Brodribb T.J., Torres-Ruiz J.M., Charra-Vaskou K., Li S., Morris H. & Jansen S. (2016) Are pine needles more vulnerable to cavitation than branches? New insights from X-ray computed tomography. *Plant, Cell and Environment* 39, 860–870.

Bouche P.S., Larter M., Domec J-C., Burlett R., Gasson P., Jansen S. & Delzon S. (2014) A broad survey of hydraulic and mechanical safety in the xylem of conifers. *Journal of Experimental Botany* 65, 4419-4431.

Brodersen C.R., McElrone A.J., Choat B., Lee E.F., Shackel K.A., Matthews M.A. (2013). In vivo visualizations of drought-induced embolism spread in *Vitis vinifera*. *Plant Physiology* 161, 1820–9.

Brodribb T.J., Bowman D.J.M.S., Nichols S., Delzon S. & Burlett R. (2010) Xylem function and growth rate interact to determine recovery rates after exposure to extreme water deficit. *New Phytologist* 188, 533–42.

Brodribb T.J. & Cochard H. (2009) Hydraulic failure defines the recovery and point of death in water-stressed conifers. *Plant physiology* 149, 575–84.

Burgess S.S.O. & Pittermann J., Dawson T.E. (2006) Hydraulic efficiency and safety of branch xylem increases with height in *Sequoia sempervirens* (D. Don) crowns. *Plant, Cell and Environment* 29, 229–239.

Charrier G., Torres-Ruiz J.M., Badel E., Burlett R., Choat B., Cochard H., Delmas C.E., Domec J.C, Jansen S., King A., Lenoir N., Martin-StPaul N., Gambetta G.A. & Delzon S. (2016) Evidence for hydraulic vulnerability segmentation and lack of xylem refilling under tension. *Plant physiology (In press)* doi: http://dx.doi.org/10.1104/pp.16.01079

Choat B., Ball M., Luly J.& Holtum J. (2003) Pit Membrane Porosity and Water Stress-Induced Cavitation in Four Co-Existing Dry Rainforest Tree Species. *Plant Physiology* 131, 41–48.

Choat B., Badel E., Burlett R., Delzon S., Cochard H. & Jansen S. (2016) Non-invasive measurement of vulnerability to drought induced embolism by X-ray microtomography. *Plant Physiology* 170, 273–282.

Choat B., Brodersen C.R. & McElrone A.J. (2015) Synchrotron X-ray microtomography of xylem embolism in *Sequoia sempervirens* saplings during cycles of drought and recovery. *New Phytologist* 205, 1095–1105. doi: 10.1111/nph.13110

Christman M.A., Sperry J.S. & Adler F.R. (2009) Testing the "rare pit" hypothesis for xylem cavitation resistance in three species of Acer. *New Phytologist* 182, 664–674.

Cochard H., Badel E., Herbette S., Delzon S., Choat B. & Jansen S. (2013). Methods for measuring plant vulnerability to cavitation: a critical review. *Journal of Experimental Botany* 64, 4779-4791.

Cochard H., Damour G., Bodet C., Tharwat I., Poirier M. & Améglio T. (2005) Evaluation of a new centrifuge technique for rapid generation of xylem vulnerability curves. *Physiologia Plantarum* 124, 410–418.

Cochard H., Torres-Ruiz J.M. & Delzon, S. (2016). Let plant hydraulics catch the wave. *Journal of Plant Hydraulics*, 3, e002. doi:http://dx.doi.org/10.20870/jph.2016.e002

Cochard H., Delzon S. & Badel E. (2015) X-ray microtomography (micro-CT): a reference technology for high-resolution quantification of xylem embolism in trees. *Plant, Cell and Environment*. 38, 201–206. doi: 10.1111/pce.12391

Cochard H., Herbette S., Barigah T., Badel E., Ennajeh M. & Vilagrosa A. (2010) Does sample length influence the shape of xylem embolism vulnerability curves? A test with the Cavitron spinning technique. *Plant, cell and environment* 33, 1543–52.

Cochard H. (2002) A technique for measuring xylem hydraulic conductance under high negative pressures. *Plant, Cell and Environment* 25, 815–819.

Dalla-Salda G., Fernández M.E., Sergent A.S., Rozenberg P., Badel E & Martinez-Meier A. (2014) Dynamics of cavitation in a Douglas-fir tree-ring: transition-wood, the lord of the ring? *Journal of Plant Hydraulics* 1, e-0005.

Delzon S. & Cochard H. (2014) Recent advances in tree hydraulics highlight the ecological significance of the hydraulic safety margin. *New Phytologist* 203, 355–358.

Delzon S., Douthe C., Sala A. & Cochard H. (2010) Mechanism of water-stress induced cavitation in conifers: bordered pit structure and function support the hypothesis of seal capillary-seeding. *Plant, Cell and Environment* 33, 2101–2111.

Dixon H.H. & Joly J. (1895) The ascent of sap. *Philosophical transactions of the Royal Society of London* 186, 563–576.

Domec J-C., Lachenbruch B.L. & Meinzer F.C. (2006) Bordered pit structure and function determine spatial patterns of air-seeding thresholds in xylem of Douglas-fir (*Pseudotsuga menziesii*; Pinaceae) trees. *American Journal of Botany* 93, 1588–1600.

Hacke U.G., Stiller V., Sperry J.S., Pittermann J. & McCulloh K.A. (2001) Cavitation fatigue. Embolism and refilling cycles can weaken the cavitation resistance of xylem. *Plant Physiology* 125, 779–86.

Hietz P., Rosner S., Sorz J. & Mayr S. (2008) Comparison of methods to quantify loss of hydraulic conductivity in Norway spruce. *Annals of Forest Science* 65, 502–508.

Knipfer T., Brodersen C., Zedan A., Kluepfel D. & McElrone A. (2015) Patterns of drought - induced embolism formation and spread in living walnut saplings visualized using x-ray microtomography. *Tree Physiology* 35, 744-755.

Lamy J-B., Bouffier L., Burlett R., Plomion C., Cochard H. & Delzon S. (2011) Uniform selection as a primary force reducing population genetic differentiation of cavitation resistance across a species range. *PLoS ONE* 6, e23476.

Lens F., Tixier A., Cochard H., Sperry J.S., Jansen S. & Herbette S. (2013) Embolism resistance as a key mechanism to understand adaptive plant strategies. *Current Opinion in Plant Biology* 16, 287-292.

Martinez-Vilalta J., Cochard H., Mencuccini M., Sterck F., Herrero A., Korhonen J.F.J., Llorens P., Nikinmaa E., Nolè A., Poyatos R., *et al.* (2009) Hydraulic adjustment of Scots pine across Europe. *New Phytologist* 184, 353–364.

Mauseth J.D. (1988) *Plant Anatomy*. California, CA, USA: Benjamin/Cummings Publishing Company.

Mencuccini M. & Grace J. (1996) Hydraulic conductance, light interception and needle nutrient concentration in Scots pine stands and their relation with net primary productivity. *Tree Physiology* 16, 459-468.

Pammenter N.W. & Vander Willigen C. (1998) A mathematical and statistical analysis of the curves illustrating vulnerability of xylem to cavitation. *Tree Physiology* 18, 589–593.

Philippe M., Cuny G. & Bashforth A (2010) *Ecpagloxylon mathiesenii* gen. nov. et sp. nov., a Jurassic wood from Greenland with several primitive angiosperm features. *Plant Systematics and Evolution* 287,153–65.

Poyatos R., Aguade D., Galiano L., Mencuccni M. & Martinez-Vilalta J. (2013) Drought-induced defoliation and long periods of near-zero gas exchange play a key role in accentuating metabolic decline of Scots pine. *New Phytologist* 200, 388-401.

Rasband W.S. (2014) ImageJ. U. S. National Institutes of Health, Bethesda, Maryland, USA, 286 http://imagej.nih.gov/ij/, 1997-2014.

Rockwell F.E., Wheeler J.K. & Holbrook N.M. (2014) Cavitation and its discontents: opportunities for resolving current controversies. *Plant Physiology* 164, 1649–1660.

Salmon Y., Torres-Ruiz J.M., Poyatos R., Martinez-Vilalta J., Meir P., Cochard H. & Mencuccini M. (2015) Balancing the risks of hydraulic failure and carbon starvation: a twig scale analysis in declining Scots pine. *Plant, Cell and Environment* 38, 2575–2588.

Schenk H.J., Steppe K. & Jansen S. (2015) Nanobubbles: a new paradigm for air-seeding in xylem. *Trends in Plant Science* 20, 199–205.

Sirviö J. & Kärenlampi P. (1998) Pits as natural irregularities in softwood fibers. *Wood and Fiber Science*. 30, 27–39

Sperry J.S., Christman M.A., Torres-Ruiz J.M., Taneda H. & Smith D.D. (2012) Vulnerability curves by centrifugation: is there an open vessel artifact, and are "r" shaped curves necessarily invalid? *Plant, Cell and Environment* 35, 601-610.

Sperry J.S. & Tyree M.T. (1988) Mechanism of water stress-induced xylem embolism. *Plant Physiology* 88, 581–587.

Sperry J.S. (2013) Cutting-edge research or cutting-edge artefact? An overdue control experiment complicates the xylem refilling story. *Plant Cell and Environment* 36, 1916-1918.

Sterck F.J., Martínez-Vilalta J., Mencuccini M., Cochard H., Gerrits P., Zweifel R., …, Sass-Klaassen U (2012) Understanding trait interactions and their impacts on growth in Scots pine branches across Europe. *Functional Ecology*, 26, 541–549.

Stiller V. & Sperry J.S. (2002) Cavitation fatigue and its reversal in sunflower (*Helianthus annuus* L.). *Journal of Experimental Botany* 53, 1155–61.

Torres-Ruiz J.M., Cochard H., Mayr S., Beikircher B., Diaz-Espejo A., Rodriguez-Dominguez C.M., Badel E. & Fernández J.E. (2014) Vulnerability to cavitation in *Olea europaea* current-year shoots: further evidence of an open-vessel artifact associated with centrifuge and air-injection techniques. *Physiologia Plantarum* 152, 465-474.

Torres-Ruiz J.M., Diaz-Espejo A., Morales-Sillero A., Martín-Palomo M.J., Mayr S., Beikircher B. & Fernández J.E. (2013) Shoot hydraulic characteristics, plant water status and stomatal response in olive trees under different soil water conditions. *Plant and Soil* 373, 77–87.

Torres-Ruiz J.M., Jansen S., Choat B., McElrone A.J., Cochard H., Brodribb T.J., Badel E., Burlett R., Bouche P.S., Brodersen C.R., Li S., Morris H. & Delzon S. (2015) Direct X-

Ray Microtomography Observation Confirms the Induction of Embolism upon Xylem Cutting under Tension. *Plant Physiology* 167, 40-43. doi: 10.1104/pp.114.249706.

Tsuda M. & Tyree M.T. (1997) Whole-plant hydraulic resistance and vulnerability segmentation in *Acer saccharinum. Tree Physiology* 17,351–357.

Tyree M.T., Cochard H., Cruiziat P., Sinclair B. & Ameglio T. (1993) Drought-induced leaf shedding in walnut: evidence for vulnerability segmentation. *Plant, Cell and Environment* 16, 879–882.

Tyree M.T. & Sperry JS. (1989) Vulnerability of xylem to cavitation and embolism. Ann Rev *Physiology and Molecular Biology of Plants* 40, 19–38.

Tyree M.T. & Zimmermann M.H. (2002) Xylem structure and the ascent of sap. Berlin: Springer.

Urli M., Porté A.J., Cochard H., Guengant Y., Burlett R. & Delzon S. (2013) Xylem embolism threshold for catastrophic hydraulic failure in angiosperm trees. *Tree Physiology* 33, 672–683.

Wheeler J.K., Huggett B.A., Tofte A.N., Rockwell F.E., Holbrook N.M. (2013) Cutting xylem under tension or supersaturated with gas can generate PLC and the appearance of rapid recovery from embolism. *Plant, Cell and Environment* 36, 1938–1949.

Zimmermann M.H & Brown C.L. (1971) Trees: structure and function. New York, NY, USA; Berlin, Heidelberg, Germany: Springer-Verlag.
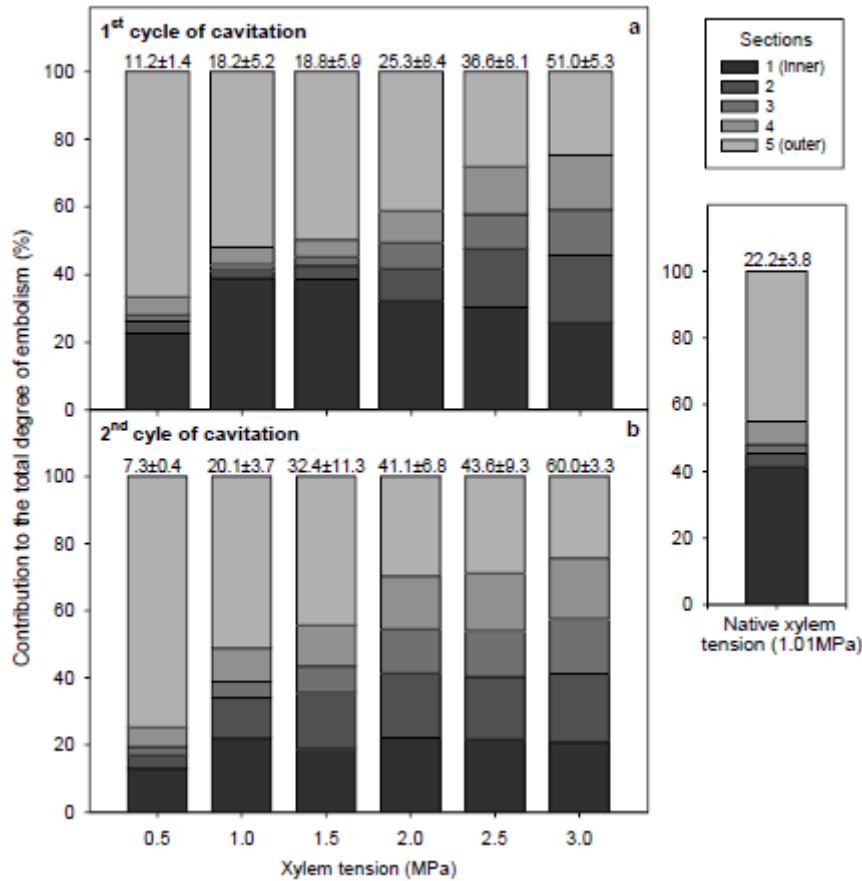
**Figure 1.** Mean contribution of each xylem section to the total degree of embolism observed at each xylem tension during the first **(a)** and the second **(b)** cycle of embolism. Panel '**c**' indicates the same but at the moment of the sample collection at their native xylem tension. Values at the top of each column indicate the mean degree of embolism (%) ± standard error observed at each tension for the entire sample. *n*=3. More details about the cycles of embolism are given in the text.
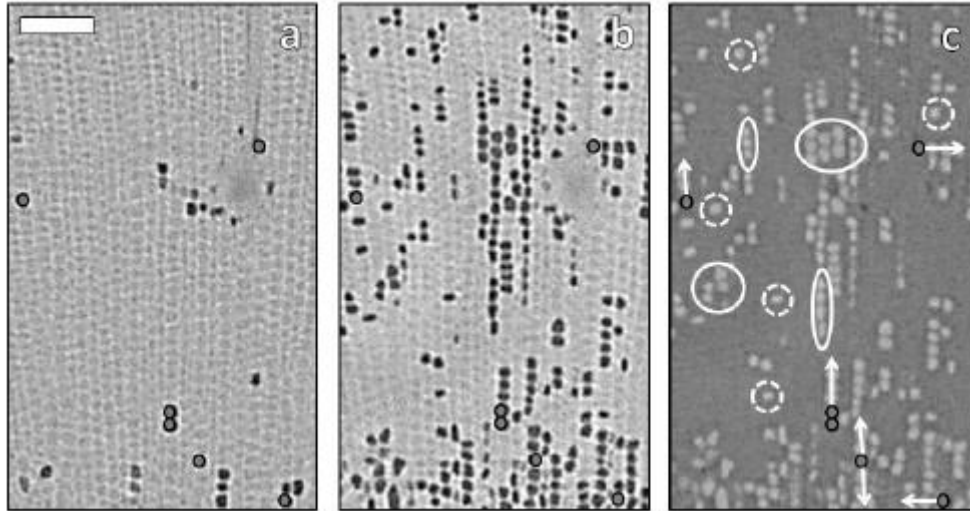
**Figure 2.** Visualization of *Pinus sylvestris* xylem tissue by X-ray microtomography (micro-CT) during the first cycle of embolism after inducing xylem tensions of 2.0 **(a)** and 2.5MPa **(b)**. Black dots indicate the embolised tracheids. Panel at the bottom **(c)** is the image resulting from the comparison of images 'a' and 'b'. It highlights the tracheids that became embolised during the xylem tension increment and evaluates the embolism spread (white dots). Grey circles with black outline indicate the tracheids already embolised at 2.0 MPa. White arrows represent the direction of embolism spread, both radially and tangentially, when xylem tensions increased from 2 to 2.5 MPa. Ellipses indicate the occurrence of both grouped (solid curves) and isolated embolised tracheids (dashed curves). Scale bar=100 μm for all the scans.

**Figure 3.** Transverse (a) and tangential (b) X-Ray microtomography images in *Pinus sylvestris* branches showing apparently isolated embolised tracheids (Tracheids #1, #2 and #3); (c) 3D re-constructed image showing how some of the isolated embolised tracheids were actually not connected to any other embolised conduits (Tracheids #1 and #3) while other apparently isolated tracheids are in fact connected at a different transversal level (Tracheid #2).
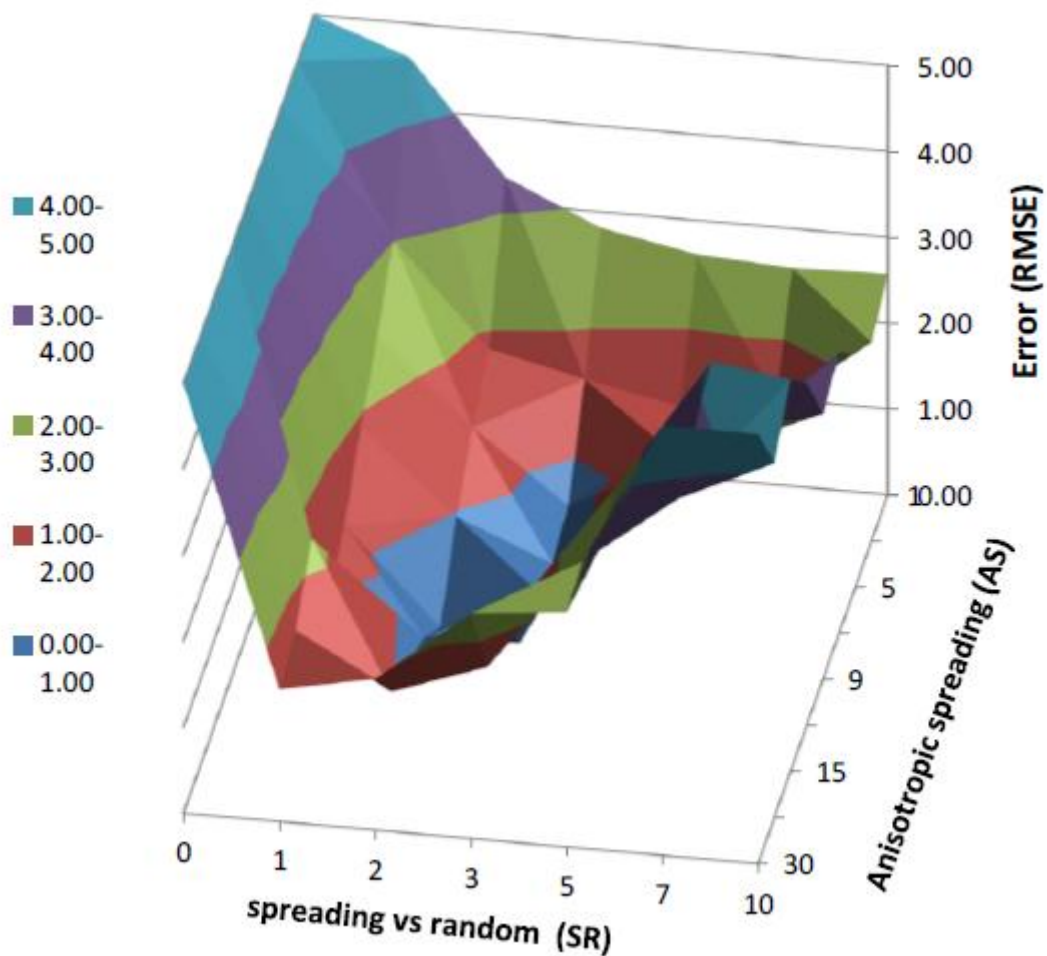
**Figure 4**: Parameterization of the model. Embolism spreading simulations were compared with direct embolism observations obtained by using X-ray microtomography (both showing 30% embolism). The fitting between the images was computed by calculating the root-mean-square error for different SR and AS given values. SR represents the ratio of the probability of spreading vs the probability of spontaneous embolism. AR represents the anisotropic ratio between the radial and tangential directions.
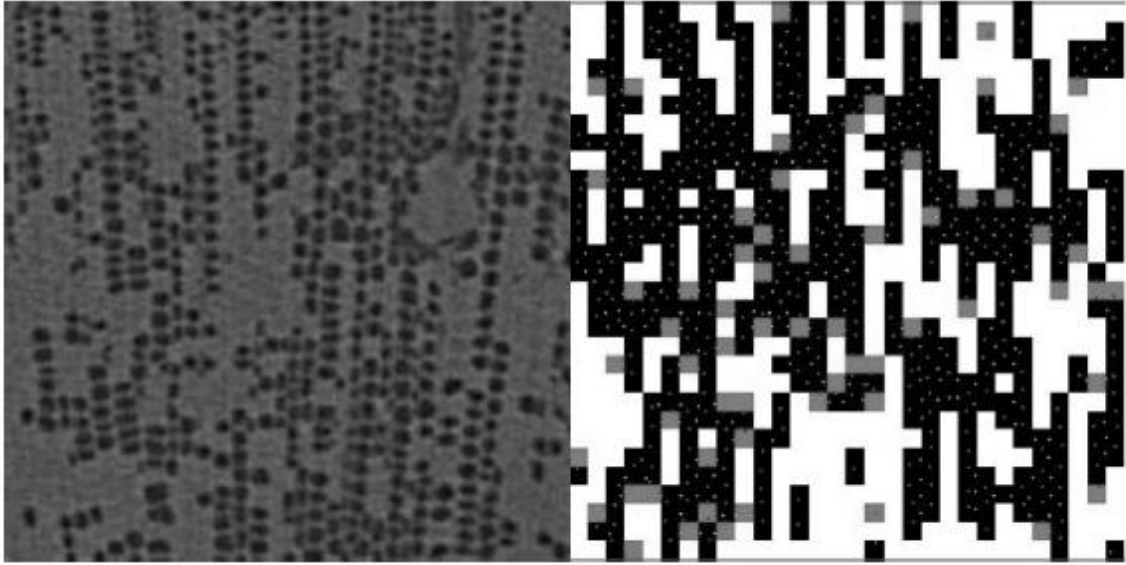
**Figure 5**: Comparison between the embolism spreading observed by X-ray microtomography (left) and the simulated ones (right). Both represent the 60% embolism. Small grey dots on the right panel represent the connections between cells. Black cells are the embolised cells. Grey cells represent the cells that become embolised at the next step.
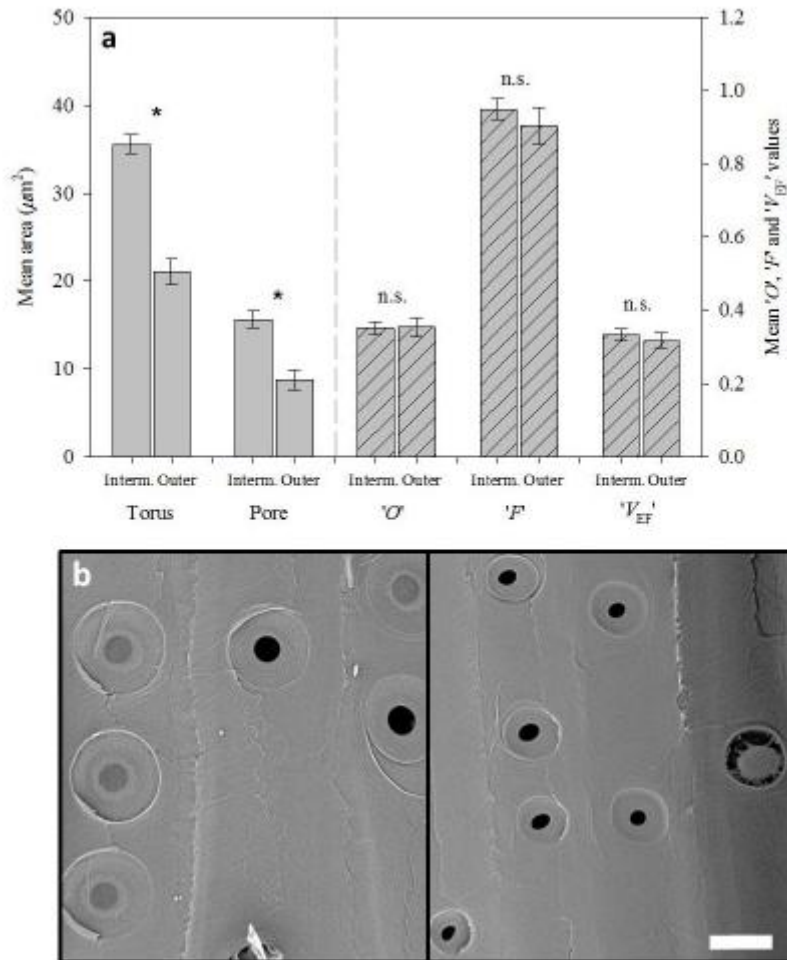
**Figure 6 (a)** Mean torus and pore aperture areas ($\mu m^2$), and calculated torus overlap ($O$), margo flexibility ($F$) and valve effect ($V_{EF}$) values for the outer (section 5) and intermediate (sections 2, 3 and 4) xylem sections (see text for details). Columns indicate means values of four different samples $\pm$ standard error. A minimum of 60 bordered pits were analysed per sample (30 located in intermediate xylem sections and 30 in the outermost one). Asterisks indicate statistically significant differences ($p < 0.05$) between xylem regions. n.s. no significant difference; **(b)** Radial views of *Pinus sylvestris* pit membranes, with and without porous margo, obtained by scanning electron microscopy (SEM) from the intermediate xylem sections (left panel) and from the outermost one (i.e. near the bark; right panel). Scale bars=10 $\mu$m for both images.
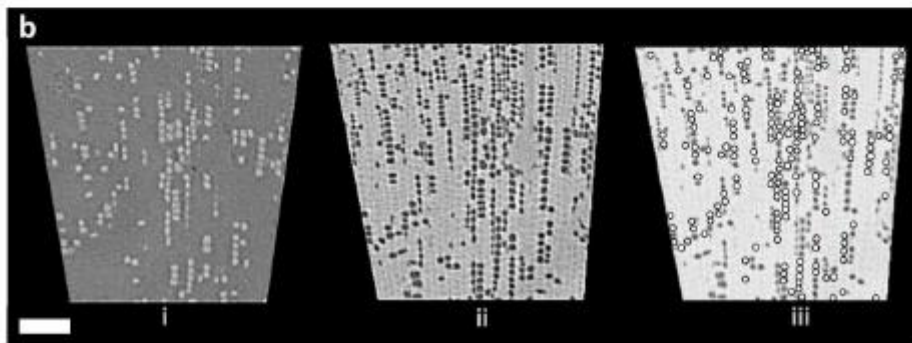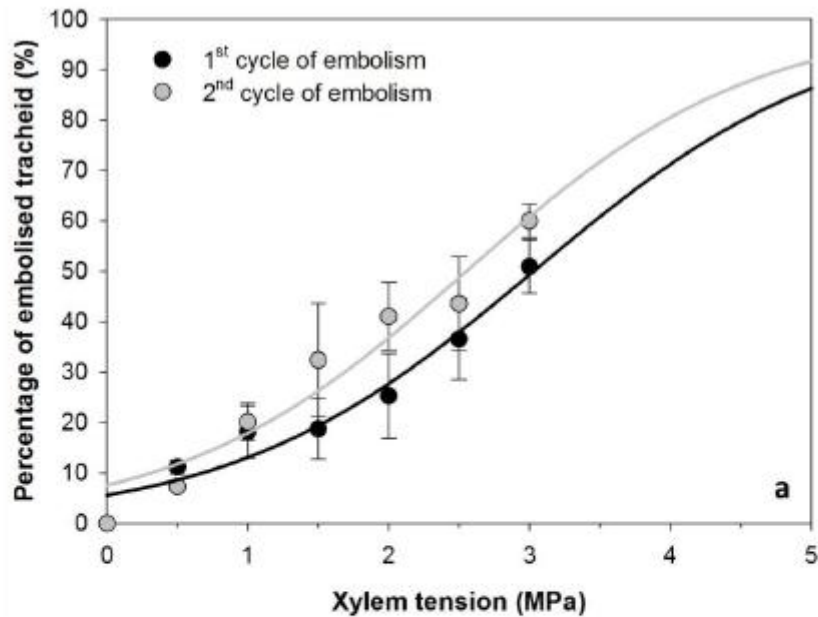
**Figure 7 (a)** Vulnerability curve generated by direct micro-CT observation from current-year Scots pine branches and after the first and second cycle of embolism (see text for details). Each point indicates the percentage of embolised tracheids by direct observation (mean ± standard error; n=3). **(b)** Visualization of the 'cavitation fatigue' phenomenon in *Pinus sylvestris* by X-ray microtomography (micro-CT). All images were obtained from the same sample and xylem region. **(i)** combined image of the scans obtained during the first cycle of embolism at xylem tensions of 2.0 and 2.5MPa to visualize only those tracheids that became embolised during this xylem tension increase (white dots); **ii)** embolised tracheids (dark dots) observed at 2.0MPa during the second cycle of embolism; and **(iii)** tracheids that became embolised at 2.0 MPa during the second cycle but which were not embolised at such tension during the first cycle (white circles with black outline). Scale bar=100 μm for all the scans.
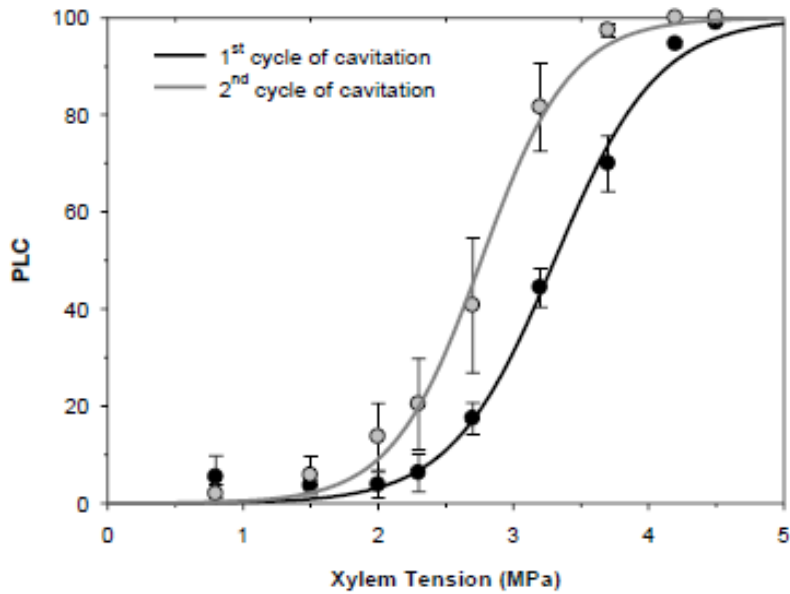
**Figure 8.** Vulnerability curves generated from current-year Scots pine branches by using the Cavitron technique. To evaluate the 'cavitation fatigue' phenomenon, all tensions were induced twice in each sample (first and second cycle of embolism, black and grey lines respectively). Each point indicates the mean degree of embolism ± standard error (*n=3*). PLC = percentage loss of hydraulic conductance.

Table 1: Xylem tensions resulting in 50% loss in conductivity (P50) or a 50% loss of functional tracheid area (50% embol.) for the first and second cycle of embolism. Each value represents the mean ± standard error ($n=3$). Asterisks indicate significant differences ($p < 0.05$) between the two embolism cycles. Details about the cycles of embolism are given in the text.

| Technique | For the entire xylem sample or portion | | For each xylem section from the inner (1) to the outer one (5) | | | | |
| | Cavitron ($P_{50}$) | Micro-CT (50% embol.) | Micro-CT (50% embol.) | | | | |
| | | | Sections: | | | | |
| | | | 1 | 2 | 3 | 4 | 5 |
| '1st cycle of embolism' | 3.30±0.07 | 2.97±0.29 | 2.24±0.49 | 3.05±0.36 | 3.33±0.02 | 3.17±0.06 | 2.23±0.51 |
| '2nd cycle of embolism' | 2.76±0.18 | 2.52±0.27 | 2.50±0.43 | 2.43±0.42 | 3.06±0.08 | 2.82±0.08 | 1.76±0.37 |
| Signif. | * | n.s. | n.s. | n.s. | * | * | n.s. |